Acta metall. Vol. 32, No. 12 pp. 2241–2249, 1984
Printed in Great Britain.

0001-6160/84 $3.00 + 0.00

FACETING OF GP ZONES IN AN Al–Ag ALLOY

K. B. ALEXANDER, F. K. LEGOUES†, H. I. AARONSON and D. E. LAUGHLIN
Department of Metallurgical Engineering and Materials Science, Carnegie-Mellon University, Pittsburgh, PA 15213, U.S.A.

(*Received* 14 *September* 1983)

Abstract—Despite observations of faceting in Al–Ag GP zones by Nicholson and Nutting in 1961 and by Gragg and Cohen in 1971, no detailed explanation for faceting was given and no systematic experimental study of the type and amount of faceting has heretofore been reported. In this paper, the faceting of GP zones in an Al–Ag alloy was investigated experimentally as a function of temperature with TEM. These observations were compared with equilibrium shape calculations obtained by using a discrete lattice plane model modified by the incorporation of thermodynamic functions appropriate to the f.c.c. Al–Ag solid solution. This model was used to calculate and plot the orientation-dependence of the chemical interfacial energy as a function of reaction temperature. Wulff constructions on these plots yielded the equilibrium shapes. A reasonably accurate accounting for the faceting and its temperature-dependence has been achieved with this approach.

Résumé—Malgré les observations anciennes du facettage des zones G.P. dans Al–Ag par Nicholson et Nutting en 1961 et par Gragg et Cohen en 1971, aucune explication satisfaisante de l'existence de ce facettage n'a été donnée et il n'y a eu aucune étude systématique de son type et de son importance. Dans cet article, nous avons étudié expérimentalement la formation du facettes sur les zones G.P. dans des alliages Al–Ag en fonction de la température. Pour cela, nous avons effectué des observations directes en microscopie électronique par transmission. Nous avons comparé ces observations avec des formes d'équilibre calculées à l'aide d'un modèle de plans réticulaires discrets, modifie pour incorporer les fonctions thermodynamiques des solutions solides AlAg c.f.c. Nous avons utilisé ce modèle pour calculer et pour tracer en fonction de l'orientation la variation de l'énergie interfaciale chimique en fonction de la température de réaction. Les constructions de Wulf sur ces tracés ont donné les formes d'équilibre. Nous avons pu rendre compte raisonnablement de la formation des facettes et de sa variation en fonction de la température.

Zusammenfassung—Trotz der frühen Beobachtung einer Facettierung von Guinier–Preston-Zonen in Al–Ag durch Nicholson und Nutting 1961 und durch Gragg und Cohn 1971 wurde bislang weder das Auftreten der Facettierung erklärt noch wurde Typ und Ausmaß untersucht. In der vorliegenden Arbeit wird die Facettierung von Guinier–Preston-Zonen in Al–Ag-Legierungen mit der elektronenmikroskopischen Durchstrahlung in Abhängigkeit von der Temperatur untersucht. Die Beobachtungen werden mit Berechnungen der Gleichgewichtsform verglichen. Für diese Berechnungen wurde ein Modell diskreter Gitterebenen durch thermodynamische, dem Al–Mg-Mischkristall angepaßte Funktionen erweitert. Mit diesem Modell wird die Orientierungsabhängigkeit der chemischen Grenzflächenenergie in Abhängigkeit von der Reaktionstemperatur berechnet. Auftragung und Auswertung mit der Wulff-Methode ergab die Gleichgewichtsform. Die Facettierung und deren Temperaturabhängigkeit wird hinreichend gut beschrieben.

1. INTRODUCTION

1.1. Aluminum–silver GP zones

The formation of Guinier–Preston zones in aluminum–silver alloys has been studied extensively since it was first recognized by Guinier [1] in 1942. Early X-ray investigations [2, 3] revealed "halos" around the transmitted and the diffracted beams. These were interpreted as arising from spherical zones in the alloys. Transmission electron microscopy [4, 5] also suggested that the zones were spherical. Laue transmission work by Geisler *et al.* [6, 7] indicated that the zones are parallel to {111} planes, leading to the suggestion that they probably represented the initial stage in the formation of plates of the transition phase γ'.

In 1971, Gragg and Cohen [8], using diffuse X-ray scattering, showed that the "halos" previously observed are actually anisotropic. They also noted that violation of "Porod's law" [9, 10] in the small-angle scattering region reported by several investigators can be explained in terms of scattering by angular volumes in the alloys. Their own careful investigation of the intensities of the diffuse scattering revealed streaking in ⟨111⟩ and ⟨100⟩ directions in reciprocal space at the fundamental nodes. From this scattering data, the Warren local ordering parameters were determined and used in a computer simulation to identify the shape of the scattering centers. Their simulations fit well with clusters that are octagonal in shape. They also reported that these zones are nearly spherical at higher temperatures. The presence of

†Present address: IBM T. J. Watson Research Center, Yorktown Heights, NY 10598, U.S.A.

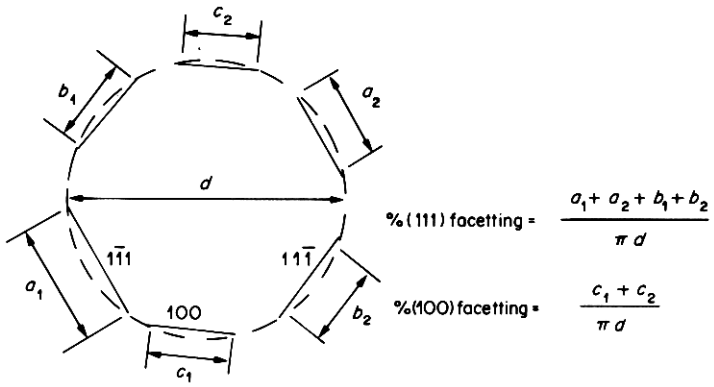

Fig. 1. Measurement technique for obtaining the percentage of faceting in the {110} section through the truncated octahedron.

faceted zones was attributed to either the better coherency provided by octahedra or to the presence of a sharp composition gradient leading to an elastic effect and a lower free energy for faceted than for perfect spheres. The latter explanation, though, necessitates assuming that the second nearest-neighbor bond energy is negative and larger than the first nearest-neighbor bond energy.

As noted by Gragg and Cohen, close examination of the transmission electron micrograph presented as Fig. 5 in the paper by Nicholson and Nutting [5] shows that the GP zones may not be perfectly spherical. Gronsky [11] has recently shown {111} facets on very small precipitates in an aluminum–silver alloy, but it is not clear that these are GP zones.

1.2. Equilibrium shape calculations

LeGoues *et al.* [12] have recently calculated the shapes of f.c.c. classical critical nuclei formed in the miscibility gap of an f.c.c. regular solid solution. In the absence of volume strain energy (which does not exceed 0.7% in the Al-rich Al–Ag alloy used in the present investigation [13]), the critical nucleus shape should be the same as the equilibrium shape. In view of the relatively high diffusivities operative [14] the shape of these zones ought to approximate quite well the equilibrium configuration.

In order to take into account the anisotropy of the f.c.c. lattice, a nearest neighbors, discrete lattice plane model was employed in conjunction with the regular solution approximation [12]. At several values of T/T_c, where T_c is the critical or maximum temperature of the regular solution miscibility gap, interfacial energy was plotted on a polar σ-plot. The Wulff construction performed on this plot yielded the equilibrium shape. At 0 K, this shape is a truncated octahedron, i.e. formed by {111} planes which are truncated by (smaller) {100} facets. At higher temperatures, the underlying spherical shape appears, decreasingly faceted by {111} and {100} planes; {111} facets are always dominant and the {100} facets disappear between 0.25 and 0.5 T_c. Above 0.5 T_c, the {111} facets also vanish and the equilibrium shape becomes a perfect sphere.

1.3. Objective of the investigation

The purpose of this study is to investigate quantitatively the faceting of GP zones in Al–Ag alloys as a function of temperature. These observations will be compared with equilibrium shape calculations similar to those of LeGoues *et al.* [12] but modified by the incorporation of thermodynamic functions appropriate to the f.c.c. Al–Ag solid solution.

2. EXPERIMENTAL

2.1. Sample preparation and examination

The alloy used in this study was Al–17.6% Ag (5.07 at.% Ag). The alloy was homogenized at 500°C and then rolled into sheet 0.020 cm thick. Individual specimens were solution annealed at 540°C for 3 hr, isothermally reacted at temperatures ranging from 160 to 350°C for times sufficient to form GP zones between 100 and 500Å in diameter and then quenched in iced water. Thin foil specimens for electron microscopy were prepared from these specimens by punching 0.3 cm discs, grinding them down to about 0.005 cm and then thinning to perforation in a twin-jet polisher using 30% nitric acid in methanol at about 10 volts at −30°C. Trace analysis having confirmed that the zones exhibited {100} and {111} facets, all further electron microscopy was performed using a ⟨110⟩ zone axis so that both types of facet could be observed edge-on simultaneously. Since the silver-rich zones are visible in the f.c.c. matrix solely by structure factor contrast, the zones were always viewed near a region where $t/\xi_g = 0.75,\ 1.75\ldots$ (t being the foil thickness and ξ_g the extinction distance), i.e. where this contrast is maximized.

2.2. Facet analysis

With the ⟨110⟩ orientation, the dimensions of the facets could be directly measured as shown in Fig. 1. As illustrated in this figure, faceting was evaluated by summing up the length of the chords of a given type of facet and dividing by the circumference that particular zone would have in the absence of faceting. Initially, the lengths of the {111} and the {100} facets on 200 different GP zones in $B = \langle 110 \rangle$ (B being the

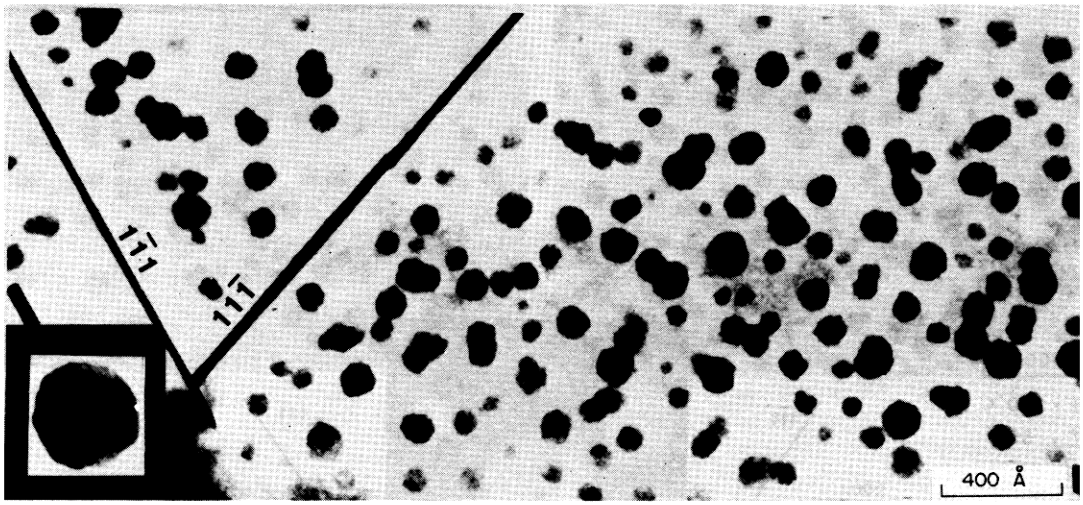

Fig. 2. Faceted GP zones in a sample aged at 160°C, $T/T_c = 0.59$. The zone axis is $B = \langle 110 \rangle$ and the traces of the {111} planes are shown on the left hand side of the figure. The small inset micrograph shows a nearly ideally faceted GP zone in Al–Ag.

zone axis) orientation were measured at each reaction temperature. However, statistical analysis showed that 60 zones was a sufficient data set; therefore, 60 zones were measured in all remaining specimens. Student t-tests and pooled t-tests were conducted on the various data sets to ascertain whether or not they were statistically different.

The theoretical faceting results obtained by utilizing the anisotropy of the interfacial energy to calculate the equilibrium shape will be presented in the same manner as the experimental results. A two-dimensional section in a (110) plane through the three-dimensional calculated shape was drawn at each temperature studied and the proportion of faceting present was computed as shown in Fig. 1. This procedure permits a direct comparison to be made between the experiments and the theory.

3. EXPERIMENTAL RESULTS

3.1. Qualitative analysis of faceted GP zones

Figure 2 is a typical illustration of faceted GP zones in the aluminum–silver alloy investigated. A few γ' plates are seen in the left-hand side of this micrograph. Note that {111} facets, i.e. those facets parallel to the γ' plates, are clearly visible. Also note that very few of the zones are perfect octagons. It was this observation that necessitated the large data sets and the subsequent statistical analysis.

Figure 3 shows GP zones at two different aging temperatures. The zones are seen to be definitely more faceted at 160°C than at 350°C.

3.2. Quantitative analysis of faceted GP zones

The proportion of faceting is shown in Fig. 4 at reaction temperatures of 160, 220, 285, 305 and 350°C. The error bars are associated with the experimental measurements and represent standard deviations. It should be noted that the {111} facet data are for two sets of facets, whereas the {100} data are for a single set of facets, because a $B = \langle 110 \rangle$ zone axis was used for quantitative analysis. The errors in the lower temperature samples are somewhat larger because of the smaller size of the zones.

Comparisons were made between the data sets using a student t-test, as well as a pooled t-test. Histograms of two sets are shown in Fig. 5. It is noted that the standard deviations associated with these data sets appear to be quite large. Student t-tests run on pairs of data sets, however, showed that the sets are different with a confidence level better than 95%. Pooled t-tests between the data sets showed similar results. These analyses are summarized in Table 1. The averages and the standard deviations obtained at the various reaction temperatures are shown in columns 2 and 3 respectively. The student t-test significance values for the data sets are given in column 4. The average of the second data set of the pairing was t-tested on the first data set. For the pooled t-test a 95% confidence interval was created for the difference of the averages of the two sets, i.e. $\bar{x}_1 - \bar{x}_2$; from this a t-test was performed to test $\bar{x}_1 = \bar{x}_2$ vs $\bar{x}_1 \neq \bar{x}_2$. The significance levels for these data sets are shown in Table 1. The amount of faceting as a function of particle size at each reaction temperature was also investigated. It was found that at a given temperature there is essentially no correlation between precipitate size and the amount of faceting.

4. THEORY

4.1. Review of the discrete lattice plane model for calculation of interfacial energy

The discrete lattice plane model has been discussed in detail and used to calculate the energy of a boundary between two f.c.c. crystals in an arbitrary

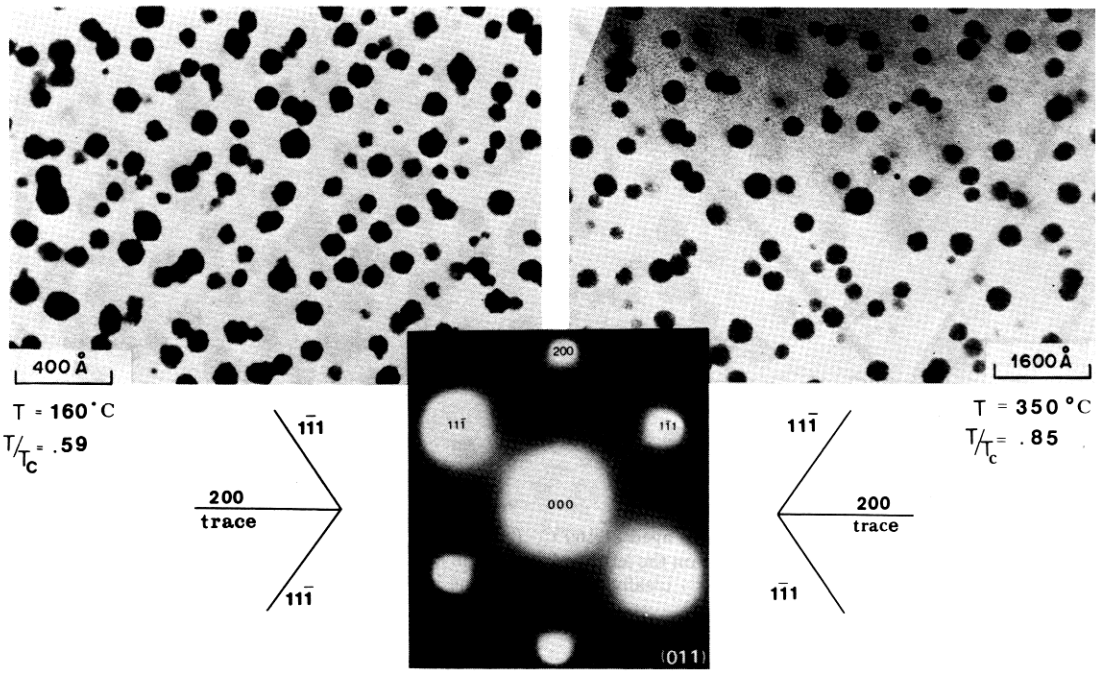

Fig. 3. The temperature-dependence of the faceting at: (a) $T = 160°C$, $T/T_c = 0.59$ and (b) $T = 350°C$, $T/T_c = 0.85$. Note that the $T = 160°C$ sample has more "angular" zones. Also note that the diffraction pattern exhibits diffuse scattering in the {111} and {100} directions around the fundamental reciprocal nodes, as previously observed by Gragg and Cohen [8].

direction in previous papers [12, 15]. The assumptions used to formulate the model are the following:

- The boundary is flat, infinite and fully coherent.
- The composition varies solely in the direction perpendicular to the boundary.
- The lattice parameter is independent of both temperature and composition.
- Only nearest neighbor interactions are taken into account.
- Both phases obey the regular solution model.

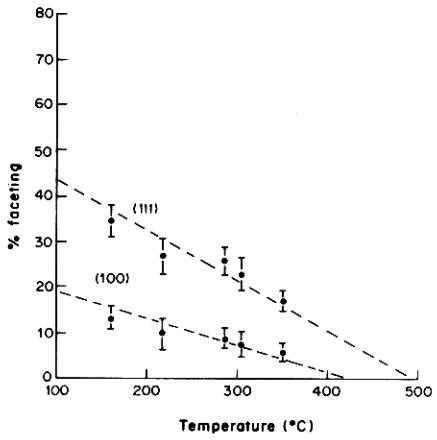

Fig. 4. Experimental results on faceting obtained using the measurement technique described in Fig. 1. The error bars are those associated with the experimental measurements and represent standard deviations.

For the present purpose, however, a more general formulation of the basic equations is needed in order to accommodate the variant of the regular solution model required by the α Al–Ag solid-solution. Cook *et al.* [16] have written a discrete lattice point version of the Cahn-Hilliard [17, 18] continuum equation for the free energy of an inhomogeneous solid solution. This relationship is equally applicable to a coherent f.c.c.:f.c.c. boundary and may be written

$$\Delta F = \frac{1}{N_v} \sum_p \left\{ \Delta F'(c_p) + \frac{K}{2a^2} \sum_r [c(p) - c(p+r)]^2 \right\} \quad (1)$$

where N_v is the number of atoms per unit volume, p is a lattice point in the inhomogeneous region, c_p is the solute concentration at p, $\Delta F'(c_p)$ is the increase in free energy at c_p relative to that of a homogeneous solid solution whose composition is given by one

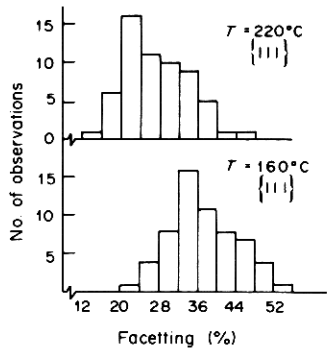

Fig. 5. Histograms for the data sets obtained for (a) $T = 160°C$, $T/T_c = 0.592$ and (b) $T = 200°C$, $T/T_c = 0.73$.

Table 1. Statistical analyses of the experimental results

Heat treatment temperature (°C)	Facet type	$\bar{x}$ $x = \%$ faceting	$\bar{\sigma}$	t-test significance value†	Pooled t-test significance value
160	{100}	13.43	3.93		
	{111}	37.47	6.69	0.000	0.000
				0.000	0.000
220	{100}	10.07	3.81		
	{111}	27.84	6.91	0.020	0.075
				0.016	0.048
285	{100}	8.9	3.28		
	{111}	25.64	4.94	0.004	0.032
				0.000	0.005
305	{100}	7.64	3.07		
	{111}	22.98	5.22	0.000	0.006
				0.000	0.000
350	{100}	5.86	3.81		
	{111}	17.04	5.4		

†The first value represents t-test done on the {100} facets, the second value represents t-test done on the {111} facets.

"arm" of the coherent miscibility gap, c_α, K is the gradient energy coefficient, a is a lattice parameter and r is the radius vector from point p to one of its nearest neighbors. If this equation is specialized to the situation of interest here, namely the variation of composition in only one direction (in which the composition of the i'th plane is uniformly c_i), it becomes

$$\Delta F = n_s \sum_i \left[\Delta F'(c_i) + \frac{\Delta E}{2} \sum_j [\{(c_{i+j} - c_i)^2 + (c_{i-j} - c_i)^2\} Z_j] \right] \quad (2)$$

where Z_j is the number of nearest neighbors that an atom in the i'th plane has in the $i+j$'th plane, n_s is the number of atoms per unit area in the i'th plane, and following Cahn and Hilliard [17] in an application of the regular solution model $K/a^2 = \Delta E$, where $\Delta E = E_{AB} - \frac{1}{2}(E_{AA} + E_{BB})$ and E_{kl} is the energy of A–B, A–A or B–B bonds, respectively. This relationship is similar to equations (20) and (40) in Ref. [15], but no longer requires that the concentration-penetration curve normal to the boundary be symmetrical. Substituting for $\Delta F'(c_i)$ a standard regular solution relationship

$$\Delta F = n_s \sum_i \left\{ kT \left[c_i \ln \frac{c_i}{c_\alpha} + (1 - c_i) \ln \frac{(1 - c_i)}{(1 - c_\alpha)} \right] + 2kT_c(c_i - c_\alpha)^2 + \frac{\Delta E}{2} \sum_j [(c_{i+j} - c_i)^2 + (c_{i-j} - c_i)^2] Z_j \right\} \quad (3)$$

where T is the absolute temperature at which ΔF is evaluated, T_c is the critical temperature of the regular solution miscibility gap, k is Boltzmann's constant and $2\,kT_c$ is the regular solution constant per atom. At equilibrium [15]

$$\frac{\partial(\Delta F)}{\partial c_i} = 0 \quad (4)$$

for all planes whose composition differs noticeably from that of either arm of the miscibility gap. Application of this condition to equation (3) yields

$$kT \left[\ln \frac{c_i(1 - c_\alpha)}{c_\alpha(1 - c_i)} \right] - 4\,kT_c(c_i - c_\alpha) + \Delta E \sum_j (c_{i+j} - 2c_i + c_{i-j}) Z_i = 0. \quad (5)$$

Equations (5) are solved simultaneously for c_i in each plane and the values are substituted into equation (3) or (2) to secure ΔF; this quantity is identically σ, the coherent chemical interphase boundary energy [17].

In Ref. [12], σ was calculated in 800 directions in the first stereographic triangle at four different temperatures. Using the symmetries of the f.c.c. lattice, this is sufficient to construct the complete σ-plot on which to perform accurately the Wulff construction, which is geometrically similar to the equilibrium shape of the minority phase. From these shapes, the percentage of {111} and {100} facets was computed as described in the Experimental Procedure section; these values are summarized in Table 2.

Comparison of Table 2 with the experimental data presented in Fig. 4 indicates that while the correct types of facet were predicted, both survive experimentally to considerably higher T/T_c's than theoretically permitted by the regular solution model. The highly asymmetric path of the GP zone solvus in the Al–Ag system [19], shown in Fig. 6, indicates that the probable source of this discrepancy lies in excessive deviations of the thermodynamics of α Al–Ag from the regular solution model. In the next section, the GP zone solvus is utilized to guide the development of a more appropriate modification of this model.

Table 2. Percentage of faceting theoretically obtained when a regular solution model is used

T/T_c	%{111}	%{100}	Total faceting
0.00	78	21	99
0.25	47	12	59
0.50	22	0	22
0.75	0	0	0
1.00	0	0	0

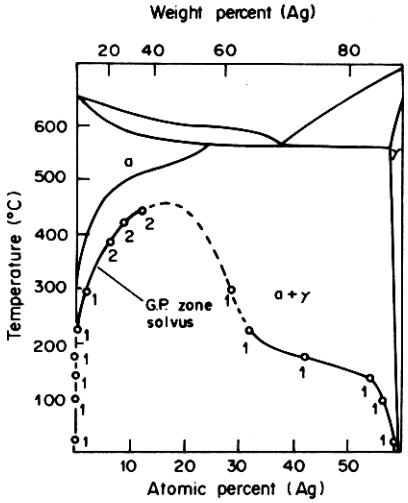

Fig. 6. Experimental phase diagram for Al–Ag (after Lorimer [1]).

4.2. Thermodynamic model

The equation chosen to model α Al–Ag thermodynamics was selected on two bases: first, an attempt was made to fit, as closely as practicable, both the GP zone solvus and the available thermodynamic data on this solid solution; second, it was necessary to keep the model as simple as possible. This second condition exists because the system of equation (4) is nonlinear and thus very difficult to solve even numerically. If the equations for $\Delta F'(c_i)$ and ΔE are too complicated, convergence problems prevent the calculation of σ in all but a few low index directions. A compromise between best fit and simplicity had thus to be found. This is why a "modified regular solution model" was used rather than a numerical best fit to the GP zone solvus. The model chosen is based on the following temperature-independent relationships

$$H^M = 8283\, c(1-c)(c-0.5)(c-1) \qquad (6)$$

$$S^M = 1.5\, k\, [c \ln c + (1-c)\ln(1-c)] \qquad (7)$$

†The nearest neighbors model is clearly in error since short range order obtains at high Ag concentrations [20], but it could not be improved upon due to the need to keep equation (4) simple.

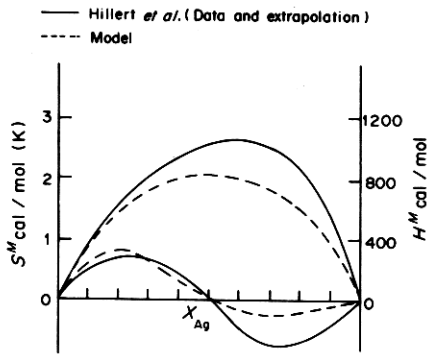

Fig. 7. Comparison of experimental thermodynamic data of Hillert *et al.* [2] with the approximations of equations (6) and (7).

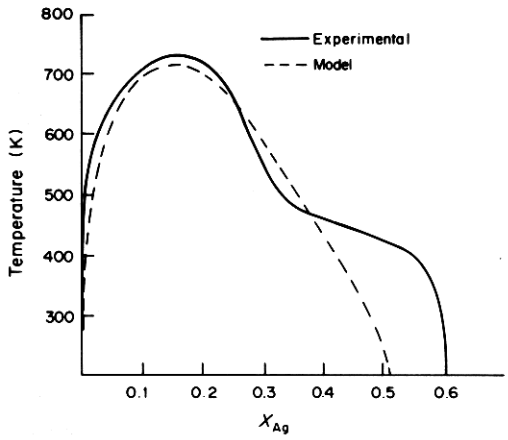

Fig. 8. Comparison of the experimental GP zone solvus with the theoretical GP zone solvus obtained by using equations (6) and (7).

where H^M and S^M are the molar enthalpy and entropy of mixing, respectively. Figure 7 shows how H^M and S^M thus computed compare with thermodynamic data determined by Hillert *et al.* [20], and Fig. 8 shows both the calculated and the experimental GP zone solvi.

It should be noted that in the equation for H^M the $(c-0.5)$ term had to be incorporated in order to fit the experimental thermodynamic data. This term implies short range order in the Ag-rich f.c.c. alloy, as noted by Hillert *et al.*, and thus explains the very asymmetric shape of the GP zone solvus. The $(c-1)$ term was added to improve the fit to the GP zone solvus. The comparison between the experimental and the theoretical GP solvi is quite satisfactory in the range of temperatures at which the experiments were performed. Using a nearest neighbors model† H^M can be written as

$$H^M = c(1-c)\frac{\Delta E}{Z} \qquad (8)$$

where Z is the bulk coordination number (12 in f.c.c.); thus

$$\Delta E = 8283\,(c-1)(c-0.5) \qquad (9)$$

ΔE now varies with composition, as expected from the thermodynamic data. Hillert *et al.* also reached this conclusion, but described a variation with composition based on Rudman's theory which is too complicated to employ in the present context.

4.3. Calculation of interfacial energy and determination of precipitate shape

Using the above thermodynamic model, equation (2) can be rewritten as

$$F = n_s \sum_i \left\{ 1.5\, kT \left[c_i \ln \frac{c_i}{c_\alpha} + (1-c_i)\ln\frac{(1-c_i)}{(1-c_\alpha)} \right] + 8283[(c_i - c_\alpha)^2(-c_i^2 - 3c_\alpha^2 + 2.5c_i + 5c_\alpha - 2c_i c_\alpha - 2)] \right.$$

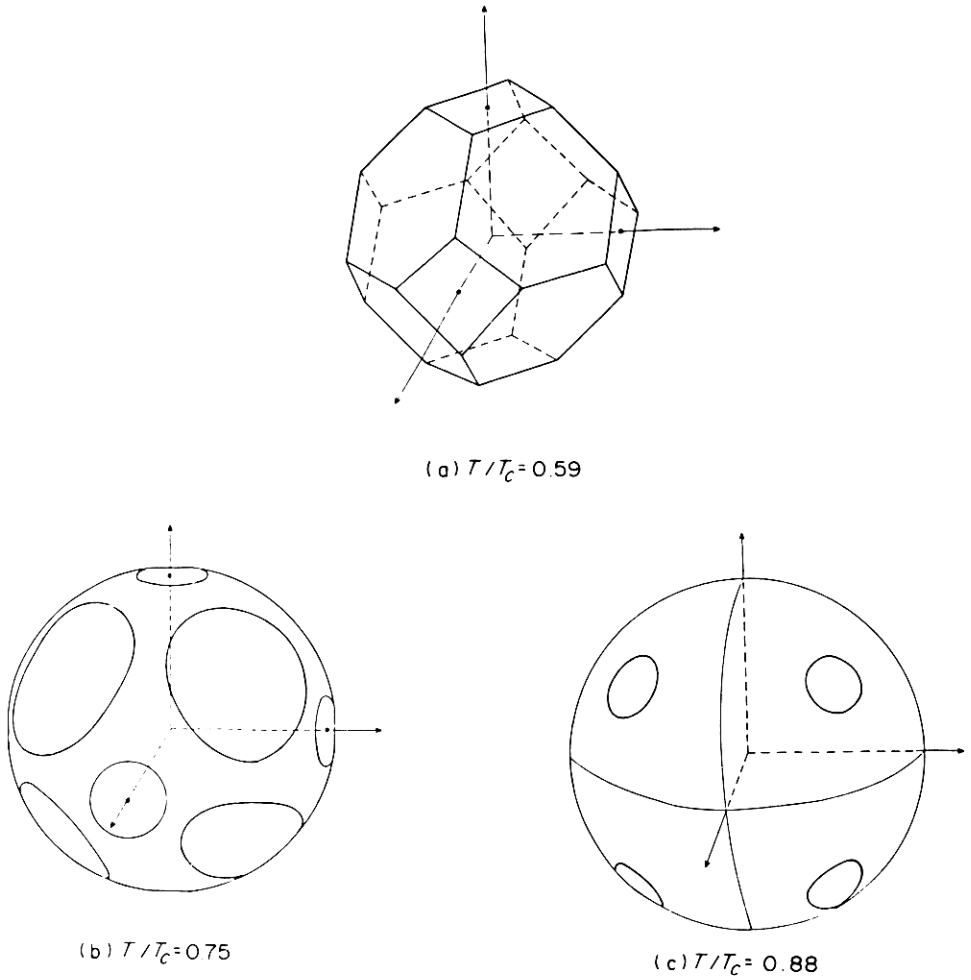

Fig. 9. Equilibrium shapes in f.c.c. Al–Ag obtained by using the discrete plane model and the thermodynamic relationships of equations (6) and (7).

$$+\frac{8283}{Z}(0.5-c_i)(1-c_i)\sum_j[(c_{i+j}-c_i)^2 + (c_{i-j}-c_i)^2]Z_j\Big\}. \quad (10)$$

Applying equation (4) yields the system of equations that must be solved to obtain the c_i's

$$8283(c_i-c_\alpha)(-4c_i^2-4c_{i\alpha}^2+7.5c_\alpha - 4c_ic_\alpha-4) - 1.5\,kT\ln\frac{c_i(1-c_\alpha)}{c_\alpha(1-c_i)} + \frac{8283}{2Z}\sum_j Z_j\{(2c_i-1.5)[(c_{i+j}-c_i)^2+(c_{i-j}-c_i)^2] - 2(0.5-c_i)(1-c_i)(c_{i+j}-2c_i+c_{i-j})\}=0 \quad (11)$$

σ was calculated at ten temperatures between 0.4 T_c and T_c in 20–50 directions of the first stereographic triangle. Because of the complexity of the system of equations and convergence problems, σ could not be computed in high index directions. Nonetheless, by extrapolation and comparison with the results obtained using the regular solution model, it was possible to construct, with fair accuracy, the complete σ-plot and thus the equilibrium shapes.

Figure 9 shows the shapes obtained at three different temperatures and Table 3 presents the percentage of faceting on the modified regular solution shapes. Note from comparison of Tables 2 and 3 that the facets flourish at markedly higher T/T_c's when the modified regular solution model is employed.

5. DISCUSSION

5.1. Comparison between theory and experiment

The theoretical predictions of faceting, using both the regular solution and the modified regular solution models, are shown in Fig. 10, together with a re-

Table 3. Percentage of faceting theoretically obtained using the modified regular solution model

T/T_c	%{111}	%{100}	Total faceting
0.50	78	21	99
0.60	63	16	79
0.70	46	9	55
0.80	30	3.5	33.5
0.90	12	0	12
1.00	0	0	0

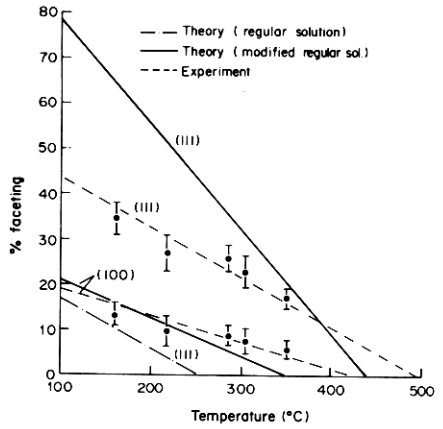

Fig. 10. Theoretical results on faceting obtained using both the regular solution model and the modified regular solution model and summary of the experimental data on faceting.

production of the experimental data. Considering first the predictions of the modified regular solution theory, it can be seen that the {100} faceting predicted and observed are in close accord. Agreement for {111} facets is predominantly qualitative, with adequate agreement primarily as to the temperature range in which faceting occurs. The discrepancies between theory and experiment can be explained by two factors. First, the thermodynamic model used is clearly too simple; it does not model the GP solvus line exactly and does not take into account second nearest neighbor interactions, which are obviously important in this alloy system [20]. Second, the measurements of the facet lengths are difficult because the edges are not always well defined. Thus, there is a tendency to underestimate the real length of the facets.

The regular solution predictions, also shown in Fig. 10, consistently underestimate the percentage of {111} facets and indicate that {100} facets are nonexistent in the range of temperatures experimentally studied. The experimental results are clearly in serious disagreement with this set of predictions.

5.2. Discussion of the differences in faceting predicted by the regular and modified regular solution models

The strong difference in anisotropy obtained when using the regular and modified regular solution models can be explained as follows. The anisotropy of the interfacial energy results from anisotropy in the number of "broken bonds" or more precisely, "bonds changed from A–A type (or B–B type) to A–B type". If we consider the problem at 0 K, when the entropy of the solution is equal to zero, the only term in the interfacial energy arises from the change in energy when exchanging an A–A or a B–B bond for an A–B bond. As shown by Lee and Aaronson [15], under these conditions

$$\sigma = n_s K \sum_j j Z_j. \tag{12}$$

Comparing, for example, the interfacial energy in the ⟨111⟩ and the ⟨100⟩ directions, we obtain

$$\text{for } \langle 100\rangle\text{: } n_s = \frac{2}{a^2} \quad Z_1 = 4, \text{ all other } Z_i = 0 \tag{13}$$

$$\text{for } \langle 111\rangle\text{: } n_s = \frac{4(3)^2}{3a^2} \quad Z_1 = 3, \text{ all other } Z_i = 0 \tag{14}$$

thus

$$\sigma^{\langle 100\rangle} = \frac{8K}{a^2} \quad \sigma^{\langle 111\rangle} = \frac{4(3)^2 K}{a^2} \tag{15}$$

hence

$$\frac{\sigma^{\langle 111\rangle}}{\sigma^{\langle 100\rangle}} = 0.860.$$

This example illustrates the strong anisotropy in the value of σ at 0 K. At higher temperatures, an entropy term is added to σ of the form

$$\Delta S = n_s \sum_i kT \left\{ c_i \ln \frac{c_i}{c_\alpha} + (1 + c_i) \ln \frac{(1 - c_i)}{(1 - c_\alpha)} \right\} \tag{16}$$

and an enthalpy term in the form

$$\Delta H = n_s \sum_i [-\Delta E (c_i - c_\alpha)^2 Z]. \tag{17}$$

Neither of these additions depends on the direction, but the gradient term is "weighted" by the diffuseness of the interface. For the ⟨111⟩ direction, for example, the gradient term becomes (in the regular solution case)

$$n_s K \sum_i (c_i - c_{i+1})^2 \times 3 \tag{18}$$

where 3 is the number of "broken bonds" in this case and $(c_i - c_{i+1})^2 < 1$ and decreases as T increases. Thus, with rising temperature the relative importance of the gradient term, i.e. of the number of "broken bonds", which is the only direction-dependent one in the equation for σ, is decreased. These considerations are valid for all thermodynamic models; however, for a regular solution model

$$K = \text{constant} = \frac{2\,kT_c}{12} = 0.1667\,kT_c \tag{19}$$

and for the modified regular solution model

$$K = \frac{5.83\,kT_c(0.5 - c)\,(1 - c)}{12} \tag{20}$$

in this case the boundary is not symmetric and K has a different value on each side of the boundary. For example, at $T/T_c = 0.5$, $c_\alpha = 0.00587$, $c_\beta = 0.441$ and thus $K_\alpha = 0.2387\,kT_c$ and $K_\beta = 0.0160\,kT_c$. K, the gradient term determines the "steepness" of the concentration profile at the interphase boundary; thus, on the K_β side of the boundary, the concentration profile will be much steeper than in the regular solution model case, even at much higher T. Thus, the "weighting" will not have as large an effect in this case and the crystallography will remain important at higher temperatures.

5.3. Discussion of the assumptions

In the comparisons between theory and experiment, we have assumed that the observed precipitates represent reasonable approximations of equilibrium shape, i.e. that can be directly compared with the theory presented here. The equilibrium shape is obtained, in principle, during nucleation and coarsening. During growth, the boundary mobility is generally taken to be negligible perpendicular to planar interfaces, and growth kinetics, therefore, depends upon the spacing between ledges present at the interface [21, 22]. Thus, growth shapes are generally determined by kinetic restrictions and can be very different from the equilibrium shape, which is controlled by interfacial energy minimization. However, in the case of coherent f.c.c. precipitates in an f.c.c. matrix (with neither phase exhibiting long-range order), there seems to be no reason to have slow growth in the direction perpendicular to a flat interface since the structure is the same on each side of the interface [23]. Additionally, the lattice strain at the interface is negligible since the lattice parameters of the zones and the matrix are virtually identical [13]. Hence faceting in this situation must have derived from interfacial energy minimization. The experimental finding that at a constant isothermal reaction temperature there was no variation in the amount of faceting as a function of either reaction time or precipitate size strongly supports the conclusion that the observed shapes adequately approximated the equilibrium ones.

6. SUMMARY

Faceting of GP zones in an Al–17.6 wt% Ag alloy was studied as a function of temperature from 160 to 350°C. It was shown that the facets were of the {111} and {100} types and that a strong temperature dependence of the proportion of the interfacial area occupied by each type of facet exists. These findings were compared with theoretical results obtained by LeGoues *et al.* [12] in which a regular solution, discrete lattice plane model [15] was used to secure the directional dependence of the interfacial energy of f.c.c. precipitates in an f.c.c. matrix, and thus the equilibrium shapes through Wulff constructions on σ-plots. Qualitative agreement between this theory and the experimental data on faceting was found, but the range of temperatures in which the variation in the amount of faceting occurred was definitely in error. This was explained by the strongly "non-regular" shape of the GP zone solvus in the Al–Ag system. In order to incorporate this behavior in the treatment, a modified regular solution model was developed to fit the GP solvus line and available thermodynamic data on f.c.c. Al–Ag alloys and substituted into the discrete lattice point model for calculating the interfacial energy. Much better agreement between theory and experiment was then found. The difference between the results obtained using the regular and the modified regular solution models is explained in terms of the broken bond model and the modification of the "weighting" factor arising from the change in the gradient energy term.

Acknowledgements—Appreciation is expressed to the Division of Materials Research of the National Science Foundation for the support of contributions to this research through Grant DMR-80-07567 for F. K. LeGoues and H. I. Aaronson and Grant DMR-81-5090 for K. B. Alexander and D. E. Laughlin.

REFERENCES

1. A. Guinier, *J. Phys. Radium, Paris* **8,** 124 (1942).
2. C. B. Walker and A. Guinier, *Acta metall.* **1,** 568 (1953).
3. V. Gerold, *Z. Metalk.* **46,** 623 (1955).
4. E. J. Freise, *Acta metall.* **9,** 250 (1961).
5. A. H. Kelly and R. B. Nicholson, *Acta metall.* **9,** 332 (1961).
6. A. H. Geisler, C. S. Barrett and R. F. Mehl, *Trans. Am. Inst. Min Engrs* **10,** 765 (1943).
7. A. H. Geisler, C. S. Barrett and R. F. Mehl, *Trans Am. Inst. Min. Engrs* **11,** 765 (1941).
8. J. L. Gragg and J. B. Cohen, *Acta metall.* **19,** 507 (1971).
9. V. Gerold, H. Auer and W. Merz, *Adv. X-Ray Analysis* **7,** 1 (1964).
10. H. Auer and V. Gerold, *Z. Metalk.* **56,** 240 (1965).
11. R. Gronsky, *Proc. Fortieth Ann. EMSA Meet.* (Edited by G. Bailey), p. 500 Claitor's, Baton Rouge, LA (1982).
12. F. K. LeGoues, H. I. Aaronson, Y. W. Lee and G. J. Fix, *Proc. Int. Conf. on Solid-Solid Phase Transformations* (edited by H. I. Aaronson, D. E. Laughlin, R. F. Sekerka and C. M. Wayman), p. 427. Metall. Soc. A.I.M.E., Warrendale, PA (1983).
13. W. B. Pearson, *Handbook of Lattice Spacings and Structures of Metals and Alloys.* Pergamon Press, Oxford (1958).
14. D. Turnbull and H. N. Treaftis, *Acta metall.* **5,** 534 (1957).
15. Y. W. Lee and H. I. Aaronson, *Acta metall.* **28,** 539 (1980).
16. H. E. Cook, D. deFontaine and J. E. Hilliard, *Acta metall.* **17,** 765 (1969).
17. J. W. Cahn and J. E. Hilliard, *J. chem. Phys.* **28,** 258 (1958).
18. J. W. Cahn and J. E. Hilliard, *J. chem. Phys.* **31,** 539 (1959).
19. G. W. Lorimer, *Precipitation Processes in Solids* (edited by K. C. Russell and H. I. Aaronson), p. 87. T.M.S.-A.I.M.E., Warrendale, PA (1976).
20. M. Hillert, B. L. Averbach and M. Cohen, *Acta metall.* **20,** 765 (1956).
21. H. I. Aaronson, C. Laird and K. R. Kinsman, *Phase Transformations* (edited by H. I. Aaronson), p. 313. Am. Soc. Metals, Metals Park, OH (1970).
22. H. I. Aaronson, *Decomposition of Austenite by Diffusional Processes*, p. 387. Interscience, New York (1962).
23. H. I. Aaronson, *Phase Transformations*, p. II–1. Institution of Metallurgists, Chameleon Press, London (1979).